EUROFUSION WPS2-PR(16) 15726

A Kleiner et al.

Neoclassical tearing mode seeding by coupling with infernal modes in low-shear tokamaks

Preprint of Paper to be submitted for publication in Nuclear Fusion

This work has been carried out within the framework of the EUROfusion Consortium and has received funding from the Euratom research and training programme 2014-2018 under grant agreement No 633053. The views and opinions expressed herein do not necessarily reflect those of the European Commission.

Neoclassical tearing mode seeding by coupling with infernal modes in low-shear tokamaks

A. Kleiner[1], J. P. Graves[1], D. Brunetti[2], W. A. Cooper[1], F. D. Halpern[1], J. -F. Luciani[3], and H. Lütjens[3]

[1]EPFL, Swiss Plasma Center (SPC), CH-1015 Lausanne, Switzerland
[2]Istituto di Fisica del Plasma IFP-CNR, I-20125 Milano, Italy
[3]Centre de Physique Théorique, Ecole Polytechnique, CNRS, F-91128 Palaiseau Cedex, France

January 15, 2016

A numerical and an analytical study of the triggering of resistive MHD modes in tokamak plasmas with low magnetic shear core is presented. Flat q profiles give rise to fast growing pressure driven MHD modes, such as infernal modes. It has been shown that infernal modes drive fast growing islands on neighbouring rational surfaces. Numerical simulations of such instabilities in a MAST-like configuration are performed with the initial value stability code XTOR-2F in the resistive frame. The evolution of magnetic islands is computed from XTOR-2F simulations as well as analytically based on Rutherford's theory in combination with the model of resistive infernal modes. The parameter Δ' is derived and additionally, the destabilizing contribution due to a helically perturbed bootstrap current is considered. Applying this model to a MAST-like configuration, we find that coupling has a strong destabilizing effect on (neoclassical) tearing modes and is able to trigger 2/1 magnetic islands in situations when the standard NTM theory predicts stability. For large width of the magnetic island, the coupling effect from infernal modes drops, but growth is maintained by the effect of the bootstrap current.

1 Introduction

Future operation scenarios for tokamaks like ITER are the standard, advanced and hybrid scenario [1]. The latter being a scenario of particular interest also in present day tokamaks, since it allows longer sawteeth-free plasma discharges at high beta and reasonably large current [2]. The hybrid scenario is characterized by low magnetic shear in the core with a flat or weakly reversed q profile, slightly above unity, where $q > 1$ across the whole plasma. Hybrid plasmas achieve high values of $\beta_N = \langle\beta\rangle a B_T / I_p$ with $\langle\beta\rangle$ being the volume averaged normalized plasma pressure, $\beta = \langle p\rangle / (B^2/(2\mu_0))$, a the minor radius, B_T the toroidal magnetic field and I_p the plasma current. Plasmas with low shear core are also met after sawtooth crashes when the field lines are fully reconnected [3, 4].

Such toroidal, low-shear core plasmas, or plasmas with shear-free core, are susceptible to a class of pressure driven MHD modes called infernal modes [5, 6], which are related to the quasi-interchange modes described by Wesson for the special case $m = n = 1$ [7]. Infernal modes are characterized by the coupling due to toroidicity, between a fundamental harmonic, which does not need to be resonant, in the core with mode numbers (m_0, n) and its $(m_0 \pm 1, n)$ sidebands due to toroidicity. When resistivity is included, the sidebands show a tearing character on their rational surfaces where $q = (m_0 \pm 1)/n$. The perturbation due to the sidebands of the infernal mode contribute to the development of fast growing modes (neoclassical tearing modes (NTMs)) [8] which decrease plasma performance or can lead to disruptions. The linear theory of infernal modes [9] predicts islands growing up to ideal timescales. Furthermore, it has also been observed experimentally that such resistive modes are able to grow much faster than classical tearing modes [10], especially following sawtooth crashes [8, 11] where the safety factor profile is completely above unity which might be interpreted as $n > 1$ modes coupling to the strong $m = 1$ internal kink perturbation. Other examples of non-resonant infernal modes have recently been considered in Refs. [12, 13, 14].

Previous analyses of resistive infernal modes were investigated without the inclusion of the bootstrap current [6, 15]. The bootstrap current plays a crucial role in the stability of toroidal plasmas, since it has a destabilizing effect which allows for unstable NTMs in situations in which classical tearing modes would be stable. In the present work we investigate the (seed island) triggering of NTMs in low-shear plasmas focusing on the coupling to infernal modes. By including effects due to the bootstrap current we consider a destabilizing mechanism that is still maintained even if the driving effect of infernal modes on the island growth were to disappear, e.g. due to the q profile in the low-shear region moving away from a rational surface r_s where $q(r_s) = m_0/n$. This allows us to see, whether the bootstrap current is able to maintain NTMs that have been triggered with the help of infernal modes

after the contribution from the triggering mechanism becomes weak. To do this, the tearing stability parameter Δ' is derived in the presence of infernal modes, ultimately in order to calculate the strength of the coupling contribution to the evolution of the island width. These analytical results are compared with numerical simulations performed by using the initial value code XTOR-2F [16]. By carrying out simulations with and without bootstrap current, the effect of the bootstrap contribution on these infernal mode triggered NTMs can be estimated and compared with analytical predictions.

This paper is organized as follows: Section 2 introduces the physical models and gives a brief description of the linear stability of infernal modes as well as the non-linear theory of neoclassical tearing mode growth. In section 3 an analytic expression for the contribution of the infernal mode coupling to the linear and non-linear growth of a NTM is made. In section 4 this is applied to a MAST-like equilibrium and the magnetic island growth is calculated using the estimate derived in the previous section. Numerical simulations of MAST-like equilibria are performed using XTOR-2F and the numerical results are compared to the analytical results. A variation of the pressure is performed and the dependency of the saturated island width on β_N is presented.

2 Physical Model

2.1 Resistive MHD Equations

The physical model used in XTOR-2F [16] is derived from the full resistive MHD equations that result from the full Braginskii equations [17] and includes non-MHD effects like thermal transport, diamagnetism and some neoclassical effects like bootstrap current [16]. Since the main extended MHD effect of interest is that of the bootstrap current, the general model [16] providing the time evolution of the velocity field $\mathbf{v}$, magnetic field $\mathbf{B}$, pressure field p and density field ρ, used by XTOR-2F is simplified to

$$\begin{aligned}
\rho\left[\partial_t\mathbf{v}+(\mathbf{v}\cdot\nabla)\mathbf{v}\right] &= \mathbf{J}\times\mathbf{B}-\nabla p+(\nabla\nu\nabla)\mathbf{v}\,,\\
\partial_t\mathbf{B} &= \nabla\times(\mathbf{v}\times\mathbf{B})-\nabla\times\eta(\mathbf{J}-\mathbf{J_{bs}})\,,\\
\partial_t p &= -\Gamma p\nabla\cdot\mathbf{v}-\mathbf{v}\cdot\nabla p+\nabla\cdot\chi_\perp\nabla p\\
&\quad+\left[\mathbf{B}\left(\frac{\chi_\parallel}{B^2}(\mathbf{B}\cdot\nabla)p\right)\right]\,,\\
\partial_t\rho &= -\rho\nabla\cdot\mathbf{v}-\mathbf{v}\cdot\nabla\rho+\nabla\cdot D_\perp\nabla\rho\,.
\end{aligned}\tag{1}$$

In the above equations the density and the pressure are defined as $\rho = m_i n_i = m_i n_e$ $p = p_e + p_i$. The subscripts e, i denote the electron and ion species, respectively. $\mathbf{J} = \nabla\times\mathbf{B}$ is the current density field. We chose for the bootstrap current $\mathbf{J_{bs}}$ to be calculated according to the Rosenbluth model [18]. The fluid velocity is given by $\mathbf{v}$. ν is the viscosity, η the resistivity and Γ the ratio of specific heats. Resistivity is allowed to vary over the radial extension of the plasma, but is kept constant in time. The resistivity profile is chosen in a way that the equilibrium toroidal electric field is kept constant over the radius [16]. $\chi_\perp$ and $\chi_\parallel$ are the perpendicular respectively the parallel heat transport coefficients and $D_\perp$ the perpendicular diffusion coefficient.

2.2 Non-linear Stability of NTMs

Non-linear stability of the tearing mode is well described by Rutherford's theory [10], originally developed for cylindrical plasmas, predicting that the growth in the early non-linear phase is linear in time and related to increasing tearing stability parameter

$$\Delta' = \lim_{\epsilon\to 0}\frac{\psi'_{r_s+\epsilon}}{\psi_{r_s+\epsilon}}-\frac{\psi'_{r_s-\epsilon}}{\psi_{r_s-\epsilon}}\,,\tag{2}$$

which measures the jump of the eigenfunction of the global perturbation on the rational surface. Several extensions to Rutherford's model have been made to include neoclassical effects and to describe neoclassical tearing modes [19, 20]. Letting w be the magnetic island width, the modified Rutherford equation describes the growth of magnetic islands by:

$$\frac{\tau_R}{r_s}\frac{\mathrm{d}w}{\mathrm{d}t} = f_n\sum_i r_s\Delta'_i(w) = f_n r_s\Delta'_{total}\,,\tag{3}$$

where $\tau_R = \mu_0 r_s^2/\eta$ denotes the resistive time, r_s is the position of the resonant surface, $S = \tau_R/\tau_A$ is the Lundquist number, $\tau_A = 1/\omega_A = R_0/v_A$ is the Alfvén time with $v_A = B_0\sqrt{(\mu_0\rho_0)}$ being the Alfvén speed. The factor f_n comes from a change in radial transport across the island and is typically set to 1.22 or 1.66 [21]. Δ'_i are the stabilizing or destabilizing contributions to the total tearing stability parameter Δ'_{total}. These include the linear standard tearing stability parameter

$$\Delta'_0 = -2m\sqrt{g^{\chi\chi}}\Lambda\pi\cot(\Lambda\pi)\,,\tag{4}$$

with $\sqrt{g^{\chi\chi}} = 1/r_s$ and $\Lambda \approx -\frac{rq}{mq'}\frac{\mu_0}{B_\theta}j'_\parallel|_{r_s}$ [22]. Eq. (4) is obtained in a simple cylinder, and large island corrections [22, 23, 24] are also known in the literature [21]. The contribution from the bootstrap current

$$\Delta'_{bs} = -4.63\frac{q_s}{q'_s}\beta_p\sqrt{\epsilon}L_p\left(\frac{w}{w^2+w_d^2}\right)\,,\tag{5}$$

provides a well known non-linear contribution to Eq. (3), arising from the current perturbation associated with pressure flattening in the region of the island [20, 25]. The bootstrap term includes corrections for small island sizes due to transport which are given by $w_d \approx \sqrt{2L_s/k_\theta}(\chi_\perp/\chi_\parallel)^{(1/4)}$ with $L_s = q^2/(q'\epsilon)$, $k_\theta = m/r$, $L_p = -p/p'$ and $\beta_p = \langle p\rangle/[B_\theta^2/(2\mu_0)]$.

Other terms usually included in non-linear NTM analysis comprise Δ'_{GGJ} [25, 26, 27], arising from toroidal geometry effects and a polarization current term Δ'_{pol} [28]. These two contributions are much smaller than the contribution of interest to this paper, which is due to coupling to infernal modes Δ'_{inf}. In effect Δ'_{inf} replaces corrections due to geometry in Δ'_{GGJ}, and corrections due to two-fluid effects in Δ'_{pol}.

Should however the infernal mode become weak, the toroidal effects and two-fluid effects associated with infernal modes could diminish such that once again Δ'_{GGJ} and

Δ'_{pol} could play a significant role in Eq. (3). As will be seen, Δ'_{inf} also naturally contains the classical Δ' term of Δ'_0. Thus in the analysis to come, the Rutherford equation will contain only contributions from Δ'_{inf} and Δ'_{bs}. Coupling of islands to infernal modes arises due to toroidal geometry. In order to represent coupling in the modified Rutherford equation, Δ' has to be calculated from the infernal mode eigenfunctions. The eigenfunctions ψ and the growth rates $\gamma = i\omega$ have to be calculated by solving the infernal mode problem. First, this is done from the linear theory, described next, valid for small islands which occur during the linear phase of mode growth. A non-linear extension to the model is also described.

2.3 Linear Theory of Infernal Modes

The model described here constitutes the basis for the derivation of the tearing stability parameter when infernal modes are present. Infernal modes are a class of pressure driven MHD modes that occur in toroidal plasmas with low or vanishingly low magnetic shear $\hat{s} = (r/q)\,q'$ in the core (here, x' describes a derivative of x with respect to r). They can be both ideal or resistive in character. The stability threshold in resistive plasmas lies below the threshold for ideal internal modes [6]. These modes occur already at very low β_p when infinite n ballooning theory predicts stable modes. Infernal modes are characterized by an ideal mode with mode number (m_0, n) located in the core, coupled to its poloidal sidebands with mode numbers $(m_0 \pm 1, n)$. The existence of such coupled modes was predicted by Zakharov in Ref. [29]. The existence of unstable pressure driven modes, far below the ballooning stability threshold, is due to the destabilizing effect of the q profile with extended low-shear when it is close to a rational value. The coupling that occurs in this situation allows an energy transfer between the ideal mode in the core and the sideband mode, resulting in a much larger growth. When resistivity is included the sideband modes develop a tearing character on their own magnetic surfaces, which contributes to the formation of magnetic islands and enhances the growth of the m_0 main mode. The growth rate of infernal modes is larger for higher pressure and small absolute $\delta q = q_{min} - m_0/n$. The typical shape of a q profile in a situation where infernal modes arise and the parameter δq is shown in Fig. 1. Classical tearing modes grow on resistive timescales like $\gamma \sim S^{-3/5}$, whereas the scaling for infernal modes is dramatically faster with $\gamma \sim S^{-3/13}$ at the ideal stability boundary.

The dispersion relation for linear resistive infernal modes with inclusion of non-MHD effects has been derived by Brunetti et. al [9]

$$\left.\frac{\omega(\omega-\omega_i^*)}{\omega_A^2}\right|_* = \frac{n^2}{1+2q_*^2}\left[\left(\frac{\delta q}{q_*}\right)^2 + \beta_p^2 G_0 \frac{B_0 - r_s\Delta'_{inf}}{A_0 - r_s\Delta'_{inf}}\right], \quad (6)$$

with the Alfvén frequency ω_A and ion diamagnetic frequency ω_i^*. The subscript $*$ indicates that a quantity is evaluated at the transition position r_* between low shear and sheared region. The poloidal β is given by $\beta_p = p_0 q_*^2/(B_0^2\epsilon^2)(a/r_0)^4$. The closeness of the q profile to the rational value is expressed through $\delta q = q_{min} - m_0/n$. r_s is the position of the rational surface of the sideband, where $q = (m_0 \pm 1)/n$. Δ'_{inf} denotes the tearing stability parameter (Eq. (2)) at the $(m_0+1)/n$ surface for a q profile of the form

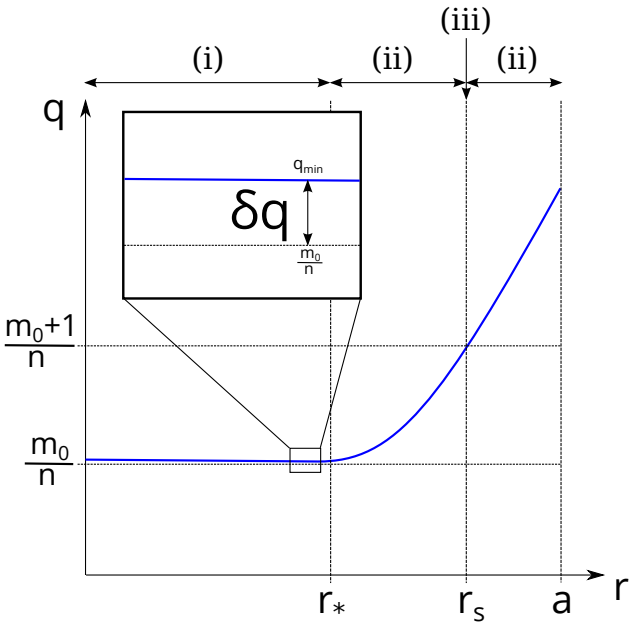

Figure 1: Typical q profile considered in the analytical theory. Region (i) is characterized by a flat q and low to vanishing shear. Region (ii) constitutes the external region in which the shear is high. The resistive layer (iii) or internal region is located at the resonant $(m_0+1)/n$ surface.

$$1/q = \iota \approx \frac{1}{m_0+1}\left\{\frac{n}{m_0}\left[1-\left(\frac{r}{r_s}\right)^{\lambda}\right]+n\right\}, \quad (7)$$

in the sheared region. The coefficients $A_0 = -\frac{\pi\cot(\pi\tilde{a})}{\lambda}(m^2-\overline{m}^2)$ and $B_0 = \pi\cot(\pi b)(m^2-\overline{m}^2)/\lambda$ carry information locally on the shape of q. Here, $\overline{m}$ is defined as $\overline{m} = \sqrt{m^2+2\lambda+\lambda^2}$, $\tilde{a} = (m-\overline{m})/\lambda$ and $b = (m+\overline{m})/\lambda$. The quantity

$$G_0 = \frac{\epsilon_*^2(r_*/r_s)^{2m}}{m(m+1)}\frac{\Gamma(\xi)\Gamma(\zeta)\Gamma(1-\xi-\zeta)}{\Gamma(-\xi)\Gamma(-\zeta)\Gamma(1+\xi+\zeta)}, \quad (8)$$

carries information about the shape of eigenfunction in terms of the q profile in the region $r < r_s$ and is written in terms of the Γ function. Setting $m = m_0+1$, $\xi = (m-\overline{m})/\lambda$ and $\zeta = (m+\overline{m})/\lambda$.

In general [9] the model includes plasma diamagnetism, subsonic equilibrium toroidal flow shear and viscosity, but these effects are not considered for this study.

3 Analytical Model for Island Width

The aim of this section is the calculation of the growth and saturated width of magnetic islands in the presence of infernal modes. Equation (3) provides the island size w with respect to time and as we have already argued should comprise Δ' contributions from infernal mode coupling

and bootstrap current, the latter having been neglected in Refs. [9, 15]. We present the calculation of Δ'_{inf}, which describes the jump of the derivative of the eigenfunction on the rational surface in the presence of infernal modes. The dispersion relation (6) has to be solved in order to obtain eigenfunction profiles, which will be needed for the linear and appropriate non-linear extended Δ'_{inf}. Additionally we consider destabilizing effects from the bootstrap current. First, this is derived for the linear phase, i.e. when the island is small. The non-linear extension for wide islands is discussed afterwards. For convenience in the following we make use of the normalized island width $\hat{w} = w/a$ and normalized time $\hat{t} = t/\tau_A$.

The plasma is split into three regions, a low-shear region in the core, a high-shear region (external region) towards the edge and a thin resistive layer (internal region) at the resonant surface, as seen in Fig. 1. The $\iota = 1/q$ profile is given by Eq. (7). The q profile that is flat in the core and results in high shear towards the edge.

By matching the eigenfunction in the resistive layer with the external eigenfunction, Δ'_{inf} calculated in the inner region can be matched to Δ'_{inf} in the outer region. A further matching of the eigenfunctions in the low-shear and high-shear regions provides the linear tearing stability parameter in presence of infernal modes

$$r_s \Delta'_{inf} = \bar{S}^{3/4} \hat{\gamma}^{5/4} \,, \tag{9}$$

where $\bar{S} = [2\pi\Gamma(3/4)/\Gamma(1/4)]^{4/3} \left[(1+2q^2)/\hat{s}_s^2\right]^{1/3} S$ with Γ being the Γ function and $\hat{s}_s$ the magnetic shear on the rational surface. The growth rate $\hat{\gamma} = \gamma/\omega_A$ is calculated from the dispersion relation of Eq. (6). Using the definition of the linear tearing stability parameter Eq. (2) Δ'_{inf} can be obtained from the eigenfunction in the external region evaluated in the limit $r \to r_s$ and a matching to the solution in the resistive layer. In the external region only the $(m_0 \pm 1, n)$ sideband contributes at leading order, while the eigenfunction of the main (m_0, n) harmonic can be neglected in that region. The sideband eigenfunctions $\xi_{r\pm}$ are governed by [9]

$$\frac{\mathrm{d}}{\mathrm{d}z}\left[z^{2/\lambda+1}(1-z)^2\frac{\mathrm{d}\xi_{r\pm}}{\mathrm{d}z}\right] - \frac{m^2-1}{\lambda^2} z^{2/\lambda-1}(1-z)^2 \xi_{r\pm} = 0 \,, \tag{10}$$

where a new radial variable $z = (r/r_s)^\lambda$ has been introduced. For ι profiles given by Eq. (7) this differential equation can be solved analytically. The eigenfunctions $\xi_{r\pm}$ describe the fluid displacement at $r < r_s$ (ξ_{r-}) respectively at $r > r_s$ (ξ_{r+}) and are given by

$$\begin{aligned}\xi_{r-} = z^{(m-1)/\lambda}(1-z)^{-1}\Big(&A_1^* F(\tilde{a}, b; \tilde{a}+b+1; z) \\ &+ B_1^* z^{-\tilde{a}-b} F(-b, -\tilde{a}; 1-\tilde{a}-b; z)\Big) \,,\end{aligned} \tag{11}$$

$$\begin{aligned}\xi_{r+} = z^{-(1+\overline{m})/\lambda}(z-1)^{-1}\Big(&A_2^* F(b, -\tilde{a}; 1+b-\tilde{a}; 1/z) \\ &+ B_2^* z^{b-\tilde{a}} F(-b, \tilde{a}; 1+\tilde{a}-b; 1/z)\Big) \,.\end{aligned} \tag{12}$$

Here, F denotes the hypergeometric function of the kind ${}_2F_1$ [30]. The fluid displacements $\xi_{r\pm}$ are related to the perturbed poloidal flux by

$$\psi_\pm = -(f_0' \hat{k}_\parallel / m) \xi_{r\pm} \,, \tag{13}$$

where $f_0' \sim r B_0$ is the radial derivative of the equilibrium toroidal flux, $\hat{k}_\parallel = m\iota - n$ is the parallel wave vector and we defined the quantities $\tilde{a} = (m - \overline{m})/\lambda$ and $b = (m + \overline{m})/\lambda$. Now, the tearing stability parameter can be written with respect to the outer eigenfunctions

$$\Delta'_{inf} = \lim_{\epsilon \to 0} \frac{\psi'_+(r_s+\epsilon) - \psi'_-(r_s-\epsilon)}{\psi_+} \,. \tag{14}$$

The external eigenfunctions, given by Eqs. (11) and (12) both consist of a regular term, describing the classical tearing behaviour and a term describing the coupling. The coefficients $A_1^*, B_1^*, A_2^*, B_2^*$ in Eqs. (11) and (12) are calculated by various boundary conditions. Ensuring the asymptotic behaviour of ξ_{r-} for $z \ll 1$ [31, 9] and making use of the above definition of Δ' gives:

$$\frac{B_1^*}{A_1^*} = -C^* \frac{A_0 - \frac{D_0}{1+D_0}(A_0 + B_0 + \overline{m}) - r_s \Delta'_{inf}}{B_0 - \frac{D_0}{1+D_0}(A_0 + B_0 + \overline{m}) - r_s \Delta'_{inf}} \,, \tag{15}$$

where $C^* = \frac{\Gamma(-\tilde{a})\Gamma(-b)\Gamma(1+\tilde{a}+b)}{\Gamma(\tilde{a})\Gamma(b)\Gamma(1-\tilde{a}-b)}$ with Γ being the Gamma function. The condition $\xi_{r+}(a) = 0$ provides an equation for the coefficient B_2^*:

$$\frac{B_2^*}{A_2^*} = -\left(\frac{r_s}{a}\right)^{2\overline{m}} \frac{F(b, -\tilde{a}; 1-\tilde{a}+b; (r_s/a)^\lambda)}{F(-b, \tilde{a}; 1+\tilde{a}-b; (r_s/a)^\lambda)} \,. \tag{16}$$

From the matching of ξ_{r-} with ξ_{r+} on the rational surface r_s we obtain

$$\frac{A_1^*}{A_2^*} = \frac{F(b, -\tilde{a}; 1+b-\tilde{a}; 1) + \frac{B_2^*}{A_2^*} F(-b, \tilde{a}; 1+\tilde{a}-b; 1)}{F(\tilde{a}, b; \tilde{a}+b+1; 1) + \frac{B_1^*}{A_1^*} F(-b, -\tilde{a}; 1-\tilde{a}-b; 1)} \,, \tag{17}$$

where the ratios $\frac{B_2^*}{A_2^*}$ and $\frac{B_1^*}{A_1^*}$ are already known from Eqs. (15) and (16). With the solution $\gamma = i\omega$ of Eq. (6) we now have all required to generate the full sideband eigenfunctions of Eqs. (11) and (12).

$\hat{\gamma}$ is plotted over δq for different values of β_p in Fig. 2. For larger β_p and low δq the mode is more unstable as expected for infernal modes. The growth rate is very large for small δq. As δq is increased the growth rate drops drastically and undergoes a transition to tearing like behaviour. This behaviour is also reflected in the linear definition of Δ'_{inf} (Eq. (14)) shown in Fig. 3 as a function of δq. The transition point appears at larger δq as β_p is increased.

The strength of the coupling is determined by the ratio B_1^*/A_1^*. In the limit of large δq, i.e. when the q profile is far from a rational value, the modes become decoupled and $B_1^* \approx 0$ due to regularity of the sideband eigenfunction on the magnetic axis. In this limit Δ'_{inf} reduces to the basic uncoupled cylindrical result of Δ'_0 given by Eq. (4). Indeed, in this case the dispersion relation becomes $r_s \Delta'_{inf} = A_0$. Using the WKB formalism the parameter

$$A_0 := 2(m_0+1)\left[-C_1\overline{C}/\left(2+2m_0+C_1\right) - \pi\Lambda\cot\left(\pi\Lambda\right)\right]$$

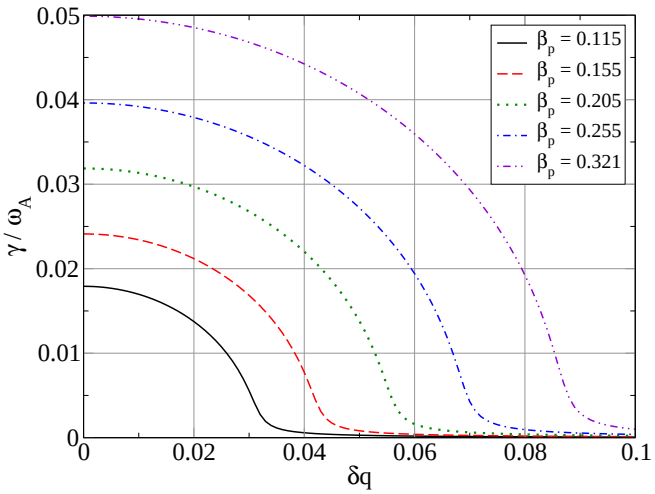

Figure 2: Dependence of the growth rate $\hat{\gamma} = \gamma/\omega_A$ on δq for different values of β_p.

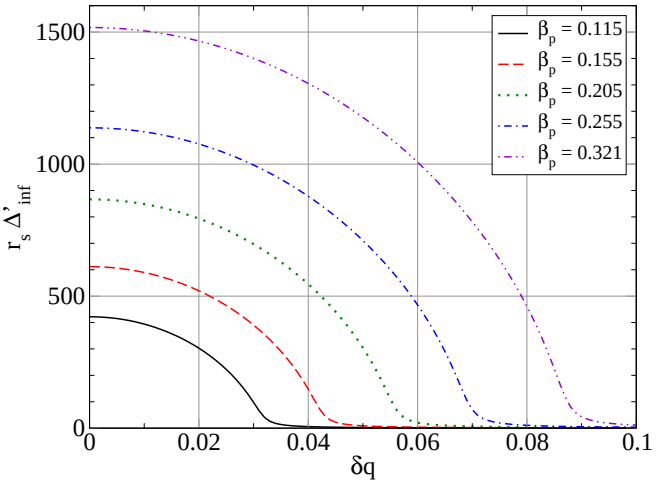

Figure 3: Dependence of the linear tearing stability parameter Δ'_{inf} calculated in presence of infernal modes on δq for different values of β_p.

with $C_1 = mr_*\iota'(r_*)/(m\iota(r_*) - n)$, $\overline{C} = \Gamma^2(1 - \Lambda)(r_*/r_s)^{2m}$ and $\Lambda = -q_s \langle R_0 J_0 \rangle'_s / (2nq'_s)$ becomes $A_0 = -2m\pi\Lambda \cot(\pi\Lambda)$ [9].

As mentioned earlier, when infernal modes are strongly unstable, Δ'_{inf} contains much more important geometric (toroidal) effects than those in Δ'_{GGJ}. In addition, Δ'_{inf} is also capable of including two-fluid effects which would dominate those in the polarization contribution. Thus, in this analysis, we consider only the effects of Δ'_{inf} and Δ'_{bs} in the modified Rutherford equation. In the linear treatment carried out so far, Δ'_{inf} is calculated in the limit $r \to r_s$. Magnetic islands of finite size affect the current profile and therefore Δ'_{inf} should be allowed to depend on w to obtain a more physically refined model. We define a finite width infernal mode contribution as [21]

$$\Delta'_{inf}(w) = \left.\frac{\psi'_+}{\psi_+}\right|_{r_s+w/2} - \left.\frac{\psi'_-}{\psi_-}\right|_{r_s-w/2}, \qquad (18)$$

where the $\psi(r)$ profile is pre-calculated in the limit of vanishing width. The importance of this correction becomes clear by looking at the external eigenfunctions, a typical example of which is shown in Fig. 4.

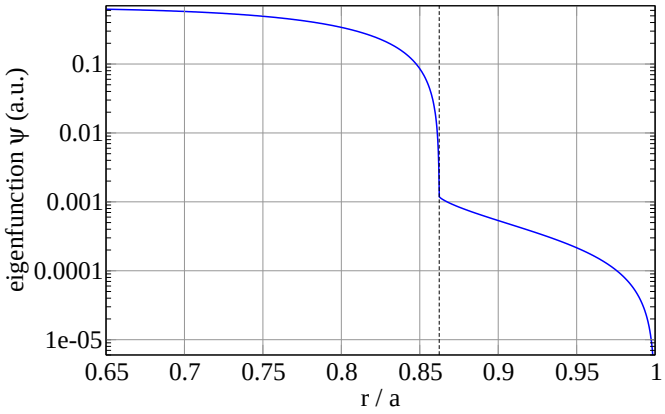

Figure 4: Sideband eigenfunction ψ in the external region (high magnetic shear) in logarithmic scale. The rational $(m_0 + 1, n)$ surface is indicated by the dashed line.

Expressing $\Delta'_{inf}(w)$ by Eq. (18) and adding the contribution from the bootstrap current, the non-linear tearing stability parameter in the presence of infernal modes can now be written as

$$\frac{\tau_R}{r_s}\frac{\mathrm{d}w}{\mathrm{d}t} = 1.66 r_s \left(\Delta'_{inf}(w) + \Delta'_{bs}\right), \qquad (19)$$

with $\Delta'_{inf}(w)$ and Δ'_{bs} given by Eqs. (18) and (5) respectively.

4 Application to a MAST-like Equilibrium

In this section the theory outlined in the previous section is applied to a MAST-like equilibrium with low-shear core. XTOR-2F simulations of the same equilibrium are presented, which have been performed with and without inclusion of bootstrap current. The results obtained by the analytical theory are compared with the results obtained by the XTOR-2F simulations.

The plasma has a major radius of $R_0 = 0.796\,\mathrm{m}$ and minor radius of $a = 0.466\,\mathrm{m}$. The resonant $q = 2/1$ surface is located at $r_s = 0.8624\,a$. The equilibrium profiles are shown in Fig. 5. The q profile is flat from the magnetic axis up to $r_s/a \approx 0.65$. We refer to this region as low shear region. For $r_s/a \geq 0.65$ finite and considerably large shear is present (high shear region). We stress the fact that Eq. (7) cannot be used to express the q profile over the whole range. Nevertheless, in the region around r_s the q profile can be approximated by $1/\iota$ with ι given by Eq. (7). The value of λ lies between 6.3 and 7 and is set to 6.7 for the following calculations.

4.1 NTM Stability Calculation with Modified Rutherford Equation

The growth of an NTM with helicity $m = 2/n = 1$ is calculated for the MAST-like equilibrium described above

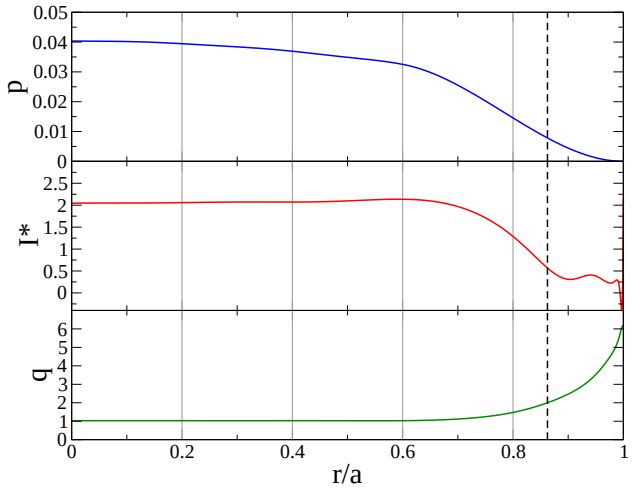

Figure 5: Equilibrium profiles of a MAST-like configuration which is susceptible to infernal modes. All profiles are plotted over $s = r/a = \sqrt{|(\psi - \psi_0)/(\psi_{edge} - \psi_0)|}$. ψ_0 is the poloidal flux on the magnetic axis. The dashed line indicates the position of the resonant $q = 2/1$ surface. p and I^* are given in CHEASE units [32].

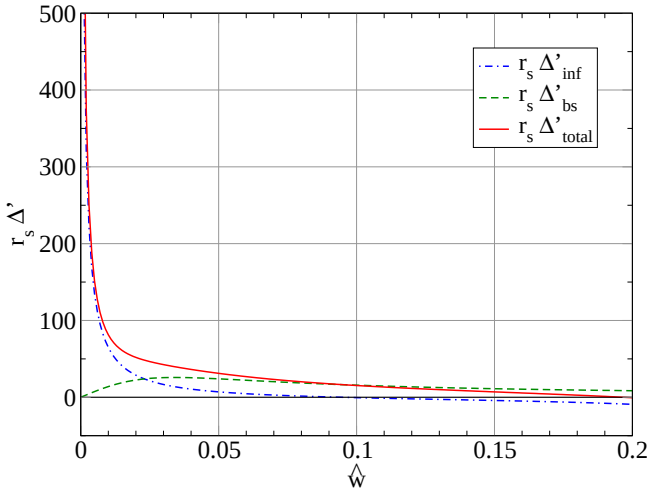

Figure 6: $\Delta'_{inf}(w)$, Δ'_{bs} and Δ'_{total} dependency on normalized island width $\hat{w} = w/a$. It is seen that the coupling term is dominant for small $\hat{w}$, whereas for increasing island width it drops and its value is comparable with the bootstrap current term Δ'_{bs}.

using Eq. (19). Cases with and without inclusion of bootstrap current are considered. In the latter case the term Δ_{bs} in Eq. (19) is set to zero. A plot of the non-linear Δ'_{inf}, Δ'_{bs} and $\Delta'_{total} = \Delta'_{inf} + \Delta'_{bs}$ is shown in Fig. 6, where calculations are obtained by solving Eq. (6). For small islands, the infernal mode coupling contribution is dominant and triggers the creation of a magnetic 2/1 island. The coupling drops very strongly as the island width increases and its magnitude becomes comparable to Δ'_{bs} for $w \gtrsim 0.03$. For very large islands the coupling term becomes stabilizing, while the bootstrap effect remains approximately constant and destabilizing.

When including the bootstrap current contribution on the island growth, we obtain a saturated island width of $\hat{w}_{sat} = 0.197$. This is larger than in the case with no bootstrap current where the island grows up to a size of $\hat{w}_{sat} = 0.095$. The saturated island widths are evaluated at the point in time where $\frac{d\hat{w}}{dt} = 0$, i.e. where $\Delta'_{total} = 0$. This analysis shows that effects from the bootstrap current can drive a magnetic island to a larger width, compared to a case when its effect is neglected.

The necessity of including coupling into the NTM stability calculations becomes obvious when Δ'_{total} is calculated in the standard way in the absence of infernal modes, i.e. by Eq. (3) complete with Δ'_{GGJ}, Δ'_{bs} and large width extensions of Δ'_0. Fig. 7 shows Δ' calculated in this way, including the non-linear tearing, GGJ and in one case bootstrap current contributions. It is seen that $\Delta'_{total}(\hat{w} = 0) < 0$ in the cases with and without consideration of bootstrap current effects. This means that the equilibrium would be (neoclassical) tearing stable and an island would not develop, contradicting numerical observations (next section) of magnetic islands in such a low-shear plasma [15].

To conclude, due to the largeness of Δ'_{inf} for $w \to 0$ the theory suggests that infernal mode coupling can provide a triggering or seeding mechanism that can lead to fast growing modes in low-shear plasmas. The destabilizing effects from the bootstrap current are able to maintain island growth to considerably larger widths than in situations where the bootstrap current is not considered.

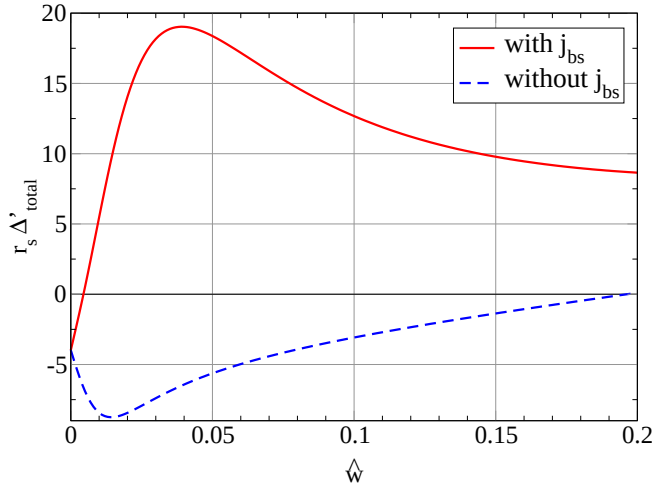

Figure 7: Δ'_{total} resulting from the standard NTM treatment, where Δ'_{total} contains cylindrical tearing, GGJ and in one case bootstrap current contributions. In both cases $\Delta'_{total}(\hat{w} = 0)$ is negative, so the island cannot grow.

4.2 Resistive Simulations

The numerical simulations are carried out with the equilibrium code CHEASE [32] which is interfaced with the initial value code XTOR-2F [16], used for the stability calculation. First, simulations are performed with the exact profiles shown in Fig. 5. Further simulations with varied pressure and current profiles enable the investigation of the effect that β_p and δq have on the growth of the side-

band magnetic island. In all the XTOR-2F simulations resistivity is included, while ion and electron diamagnetic effects are switched off. The largest poloidal mode considered in the simulations is $m = 13$ for $n = 1$. For $n = 0$ the maximum poloidal mode number is chosen for each equilibrium configuration individually such that convergence is achieved. The largest poloidal mode considered m_{sup}, lies in the range $12 \leq m_{sup} \leq 24$ for each simulation. The discretization grid consists of 201 points in radial direction, 24 points in toroidal direction and in poloidal direction of 96 points when $m_{sup} \geq 20$ and 64 points in simulations where $m_{sup} < 20$. The Lundquist number is set to $S = 10^6$ on the magnetic axis. This value is lower than the typical values for present day tokamaks (ranging from $S = 10^8 - 10^9$), but larger values in the simulation can lead to unnecessary convergence problems. Equilibrium toroidal rotation is neglected in the simulations. The resistivity is allowed to vary over the radial extension of the plasma, unlike in the analytical model, where resistivity matters only in the resonant region, where it can be considered constant. The value for the normalized viscosity is $\nu = 5 \times 10^{-6}$.

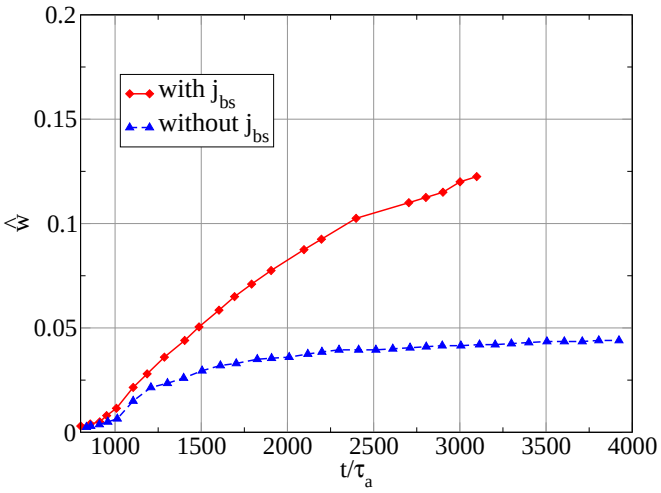

Figure 8: Island width with and without bootstrap current as computed in the XTOR-2F simulations. When bootstrap current is included, the island growths to a larger size.

First, simulations with the above equilibrium profiles are performed. The poloidal β_p for this equilibrium is $\beta_p = 0.32$ for which $\beta_N = 1.66$. Here, a 2/1 island is observed, both in the cases with and without bootstrap current. The island evolution can be seen in Fig. 8. During the linear phase which ends at $t \approx 1000\,\tau_A$ the growth of the magnetic island is exponential and comparable in both cases. For $t > 1000\,\tau_A$, when the system enters the nonlinear stage, the mode growth is stronger and maintained for a longer time in the case when bootstrap current is included. The comparable growth during the linear phase that is observed in both cases, results from the low value of Δ'_{bs}, which can be neglected for small island sizes. The difference of the growth rate in the non-linear phase is expected, since Δ'_{bs} becomes important here and has a strong destabilizing effect for larger island width.

Fig. 9 shows Poincaré plots of the poloidal cross section at toroidal angle $\phi = 0$ at $t \approx 2800\,\tau_A$, when the 2/1 islands reach significant sizes. The main 1/1 mode can also be seen, shifting the magnetic axis outward and giving the flux surfaces in the core a bean-like shape.

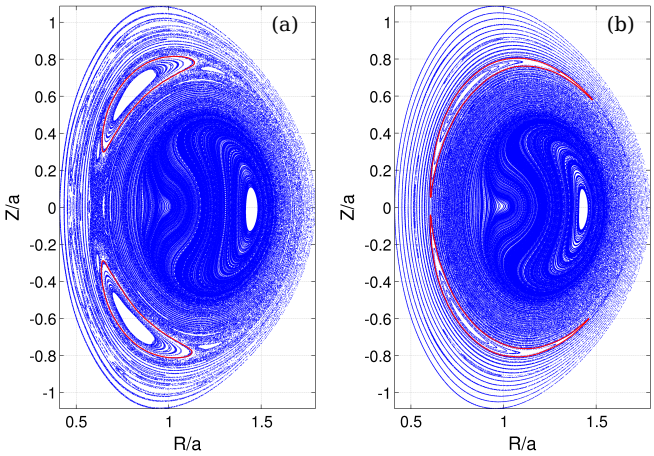

Figure 9: Poincaré plot at $\varphi = 0$ at time $t = 2480\,\tau_A$ in simulations with equilibrium profiles as in Fig. 5. The magnetic 2/1 island is clearly visible. (a) with inclusion of bootstrap current. (b) at without inclusion of bootstrap current.

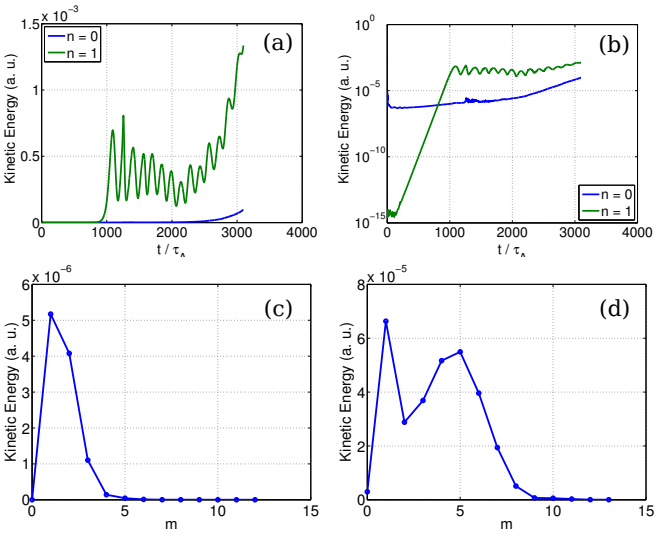

Figure 10: Kinetic energy of the $n = 0$ and $n = 1$ mode in a simulation including bootstrap current and using the equilibrium profiles seen in Fig. 5. (a) shows the energy on a linear scale, (b) on logarithmic scale. The m spectrum of the $n = 0$ mode is shown in (c) and the m spectrum of $n = 1$ mode in (d), both for $t = 2500\,\tau_A$.

The typical evolution of the kinetic energy of an infernal mode is shown in Fig. 10. The energy growths linearly until $t \approx 1000\,\tau_A$ and then enters the non-linear stage, characterized by an oscillating behaviour. The poloidal spectrum is well converged. The kinetic energy is related to the growth rate by $\gamma = -i\omega = 1/2\,\mathrm{d}\ln(E_K)/\mathrm{d}t$, where E_k is the kinetic energy of the mode and it is linked to the fluid displacement ξ by $E_{kin} = 1/2\,m\,\partial\xi/\partial t$ and therefore

allows the estimation of the mode amplitude. From the beginning of the non-linear phase the amplitude of the oscillations reduces until $t \approx 2200\,\tau_A$. After $t \approx 2200\,\tau_A$ the amplitude of the kinetic energy of the $n = 1$ mode rises notably while the oscillation frequency decreases. This is due to the effect of destabilizing effect of the bootstrap current, leading to a substantially larger island width. A similar behaviour, but without a rise of the kinetic energy at large times, is also observed in the simulations without bootstrap current.

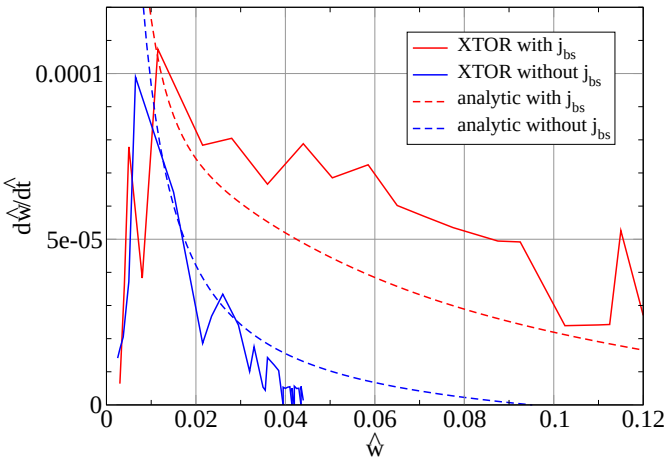

Figure 11: Island growth $\mathrm{d}\hat{w}/\mathrm{d}t$ is shown with respect to island width $\hat{w}$ for XTOR-2F simulations and the analytical prediction for cases with and without bootstrap current. Agreement between simulations and analytical results is found.

From the analysis that has been done so far, it is unclear if the islands are saturated. Saturation can be estimated by relating $\mathrm{d}\hat{w}/\mathrm{d}t$ to the width $\hat{w}$. For a non-saturated island $\mathrm{d}\hat{w}/\mathrm{d}t > 0$ and saturation is obtained when $\mathrm{d}\hat{w}/\mathrm{d}\hat{t} = 0$. The relation between island growth and width is shown in Fig. 11 for both the analytical results and XTOR-2F, with and without bootstrap current effects. In the XTOR-2F simulation without inclusion of bootstrap current saturation is achieved at a width $\hat{w}_{sat} = 0.044$. In the case with bootstrap current the island is not saturated at the end of the simulation at $t = 3098\,\tau_A$, though island growth, i.e. the slope $\dot{\hat{w}} = \mathrm{d}\hat{w}/\mathrm{d}\hat{t}$ is reduced to 1/3 of its maximal value. For small island sizes the growth of bootstrap and non-bootstrap simulations are comparable as expected.

The analytical island growth is calculated using Eq. (19). In order to compare the XTOR-2F simulations without inclusion of bootstrap current to the analytical model, the term Δ'_{bs} in Eq. (19) is set to zero for this case. For both cases the numerical and analytical results agree well. The apparent large seed island effect, where $\mathrm{d}\hat{w}/\mathrm{d}\hat{t}$ is large for small $\hat{w}$ is observed in both the analytic results and XTOR-2F. Difference between saturated values in $\hat{w}$ are likely to be due to the approximations that have been made for the non-linear corrections in the derivation of Eq. (19).

From the dispersion relation Eq. (6) it can be seen

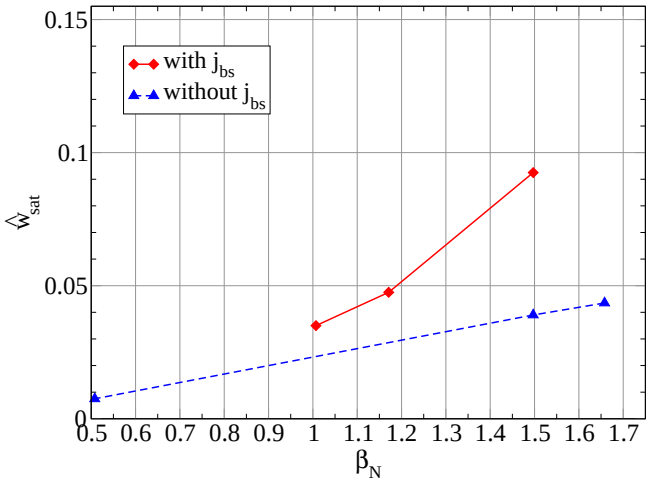

Figure 12: Saturated magnetic island width $\hat{w}$ versus pressure on the magnetic axis p_0 from XTOR-2F simulations with and without bootstrap current. Note, that the whole pressure profile is scaled down, hence not only p_0 varies, but $p(r)$ for $0 \leq r \leq a$.

that the growth rate of infernal modes depends on $\beta_p = p/(B_\theta^2/2\mu_0)$. In order to examine the influence of β_p on the growth of the 2/1 NTM, the pressure profile is scaled by multiplying $p(r)$ with a constant parameter c over the range $0.3 \leq c \leq 1$. The shape of the profile is maintained. This is done for cases with and without bootstrap current and the result is shown in Fig. 12. Without bootstrap current, there is a linear dependence on $p(r)$, which results from the effect of increasing p on the infernal mode growth rate. With the additional effect of bootstrap current, and its dependence on pressure, the island width scales non-linearly on p.

5 Conclusions

In this work analytical and numerical studies in the frame of resistive MHD with inclusion of bootstrap current have been presented. In particular we investigated the triggering of fast growing MHD modes by infernal modes in low-shear plasmas. Analytical and numerical results for cases with and without bootstrap current have been compared and good agreement has been found.

Standard NTM analysis [25] is not applicable when islands are coupled to infernal modes. In this work a derivation of the infernal mode coupling contribution to the modified Rutherford equation has been presented. To obtain the linear Δ'_{inf}, which describes the initial 'kick' that can trigger the creation of an NTM, the external eigenfunctions have been evaluated in the limit $r \to r_s$. The resulting destabilizing effect is much stronger compared to standard tearing analysis, suggesting that coupling provides the dominant destabilizing effect. A non-linear extension which evaluates Δ' at finite width has been provided to generalize the equation governing island growth.

The new analytical model has been applied to a MAST-like equilibrium with low-shear core. In such a plasma,

where infernal modes are present, the modified Rutherford equation used in standard (neoclassical) tearing theory predicts stability, even when the destabilizing term Δ'_{bs} is considered. With the new contribution Δ'_{inf} in the modified Rutherford equation, the coupling provides a strongly destabilizing effect that triggers a magnetic island. Due to the largeness of Δ'_{inf} for small widths, the island shows a very fast growth at this width. This highly destabilizing effect of coupling can explain the triggering of magnetic islands in numerical simulations and the experimentally observed fast growing modes.

Numerical simulation results obtained with the XTOR-2F code in the same equilibrium, show the existence of a fast growing 2/1 island. When bootstrap current is considered, the island grows much faster and to a larger width than in the case without bootstrap current. This behaviour is expected due to its additional destabilizing effect. A comparison with the analytical model shows good agreement for the island growth in both cases.

Acknowledgments

This work has been carried out within the framework of the EUROfusion Consortium and has received funding from the European Union's Horizon 2020 research and innovation programme under grant agreement number 633053. The views and opinions expressed herein do not necessarily reflect those of the European Commission.

This work was supported in part by the Swiss National Science Foundation.

References

[1] A. Staebler *et al.*, Nuclear Fusion **45**, 617 (2005).

[2] C. Gormezano *et al.*, Nuclear Fusion **47**, S285 (2007).

[3] B. B. Kadomtsev, Soviet Journal of Plasma Physics **1**, 389 (1975).

[4] F. Porcelli, D. Boucher, and M. N. Rosenbluth, Plasma Physics and Controlled Fusion **38**, 2163 (1996).

[5] J. Manickam, N. Pomphrey, and A. Todd, Nuclear Fusion **27**, 1461 (1987).

[6] L. A. Charlton, R. J. Hastie, and T. C. Hender, Physics of Fluids B **1**, 798 (1989).

[7] J. A. Wesson, Plasma Physics and Controlled Fusion **28**, 243 (1986).

[8] G. Canal *et al.*, Nuclear Fusion **53**, 113026 (2013).

[9] D. Brunetti, J. P. Graves, W. A. Cooper, and C. Wahlberg, Plasma Physics and Controlled Fusion **56**, 075025 (2014).

[10] P. H. Rutherford, Physics of Fluids **16**, 1903 (1973).

[11] J. P. Graves *et al.*, Nature Communications **3**, 624 (2012).

[12] J. Breslau *et al.*, Nuclear Fusion **51**, 063027 (2011).

[13] F. Wang, G. Y. Fu, J. A. Breslau, and J. Y. Liu, Physics of Plasmas **20** (2013).

[14] F. Wang, G. Y. Fu, J. A. Breslau, K. Tritz, and J. Y. Liu, Physics of Plasmas **20** (2013).

[15] D. Brunetti *et al.*, Plasma Physics and Controlled Fusion **57**, 054002 (2015).

[16] H. Lütjens and J.-F. Luciani, Journal of Computational Physics **229**, 8130 (2010).

[17] S. I. Braginskii, Reviews of Plasma Physics **1**, 205 (1965).

[18] M. Rosenbluth, D. Ross, and D. Kostomarov, Nuclear Fusion **12**, 3 (1972).

[19] R. J. La Haye, Physics of Plasmas **13**, (2006).

[20] N. N. Gorelenkov, R. V. Budny, Z. Chang, M. V. Gorelenkova, and L. E. Zakharov, Physics of Plasmas **3**, 3379 (1996).

[21] J. Wesson, *Tokamaks*, 3rd edition. ed. (OUP Oxford, New York, London, 2004).

[22] C. C. Hegna and J. D. Callen, Physics of Plasmas **1**, 2308 (1994).

[23] R. B. White, D. A. Monticello, M. N. Rosenbluth, and B. V. Waddell, Physics of Fluids **20**, 800 (1977).

[24] R. B. White, D. A. Monticello, M. N. Rosenbluth, and B. V. Waddell, Physics of Fluids **20**, 800 (1977).

[25] O. Sauter *et al.*, Physics of Plasmas **4**, 1654 (1997).

[26] A. H. Glasser, J. M. Greene, and J. L. Johnson, Physics of Fluids **18**, 875 (1975).

[27] A. H. Glasser, J. M. Greene, and J. L. Johnson, Physics of Fluids **19**, 567 (1976).

[28] H. R. Wilson, J. W. Connor, R. J. Hastie, and C. C. Hegna, Physics of Plasmas **3**, 248 (1996).

[29] L. Zakharov, Nuclear Fusion **18**, 335 (1978).

[30] M. Abramowitz and I. Stegun, *Handbook of Mathematical Functions* (Dover Publications, New York, 1965).

[31] F. L. Waelbroeck and R. D. Hazeltine, Physics of Fluids **31**, 1217 (1988).

[32] H. Lütjens, A. Bondeson, and O. Sauter, Computer Physics Communications **97**, 219 (1996).